Fluid Phase Equilibria 589 (2025) 114247

Contents lists available at ScienceDirect

Fluid Phase Equilibria

journal homepage: www.journals.elsevier.com/fluid-phase-equilibria

Co-sorption of volatile components in polymer-based pharmaceutical formulations

Jana Kerkhoff [a,b], Dominik Borrmann [a], Gabriele Sadowski [a,*]

[a] Department of Chemical and Biochemical Engineering, Laboratory of Thermodynamics, TU Dortmund University, Emil-Figge-Str. 70 D-44227 Dortmund, Germany
[b] INVITE GmbH, Drug Delivery and Innovation Center (DDIC) 51368 Leverkusen, Germany

ARTICLE INFO

Keywords:
Co-sorption
Sorption isotherm
ASDs
Raman
DVS
PC-SAFT
NET-GP

ABSTRACT

Amorphous Solid Dispersions (ASDs) are mixtures of active pharmaceutical ingredients (APIs) and polymers aiming to increase API aqueous solubility and bioavailability. ASDs are often produced using solvent-based manufacturing, such as spray drying. Due to solubility or miscibility limitations in one solvent, solvent mixtures are frequently used for this purpose. Drying solvents or solvent mixtures from polymer-based products like ASDs is an energy-intensive and time-consuming process. Designing and optimising this drying process requires knowledge of the sorption isotherms of the solvent(s) in these polymer-based products. In this work, we developed a novel approach for measuring the simultaneous absorption/desorption of two solvents in a polymer. Combining classical dynamic vapour sorption (DVS) measurements with Raman spectroscopy, this innovative approach provides a more detailed and accurate measurement of the sorption isotherms than common methods. Moreover, we developed an approach for precisely predicting the sorption equilibria in three-component systems just based on sorption data of the corresponding binary subsystems. Our modelling approach combines the Perturbed-Chain Statistical Associating Fluid Theory (PC-SAFT) with the Non-Equilibrium Thermodynamics of Glassy Polymers (NET-GP). Building on the description of the sorption isotherms of either water or ethanol in poly(vinylpyrrolidone-co-vinyl acetate) (PVPVA64) and in indomethacin (IND), we were able to quantitatively predict the simultaneous sorption of water and ethanol in PVPVA64 and the one of ethanol in an IND/PVPVA64 ASD.

1. Introduction

Knowing the sorption isotherms of solvents in polymers is crucial for designing drying processes for polymer-based products, e.g. Amorphous Solid Dispersions (ASDs), where the active pharmaceutical ingredient (API) is dissolved in a polymer. The present study uses indomethacin (IND) as a model API and poly(vinylpyrrolidone-co-vinyl acetate) (PVPVA64) as a pharmaceutically relevant polymer commonly used for ASDs. [1,2]

Standard manufacturing processes for polymer-based products like ASDs, such as spray drying or fluidised-bed granulation, use solvents in which the different ingredients are commonly dissolved. In a subsequent step, the solvent is evaporated from this solution to form a homogenous and amorphous solvent-free product. [3] However, due to solubility limitations, sometimes solvent mixtures are used for that purpose, influencing the overall drying process. [4–6] Two solvents usually have different volatilities. This means that during drying, the two solvents will certainly evaporate to a different degree, meaning that the solvent composition in the sample will change over time during drying. Moreover, the drying behaviour of a solvent is influenced by both the presence of another solvent and the composition (drug load) of the polymeric product. This cannot be treated as just an overlay of the drying behaviour of the corresponding binary subsystems.

Despite the high interest in industrial applications, only a few data for simultaneous sorption of two solvents in a polymer, API or ASD, are available. A reason for this lack of data is that measuring sorption isotherms for two-solvent systems is quite demanding. Gravimetric methods, like dynamic vapour sorption, determine the total mass of absorbed/desorbed solvent(s) as the difference between the total mass of the wet sample and the (constant) mass of the non-volatile polymer, API, or ASD. However, they cannot distinguish between two solvents within the sample. Thus, it is impossible to determine the two solvent concentrations in the polymer, API or ASD, via gravimetric methods alone.

* Corresponding author.
E-mail address: gabriele.sadowski@tu-dortmund.de (G. Sadowski).

https://doi.org/10.1016/j.fluid.2024.114247
Received 22 August 2024; Received in revised form 27 September 2024; Accepted 3 October 2024
Available online 5 October 2024

Thus, only a few studies exist that measure the sorption isotherms of two-solvent systems. Bonner et al. [7], and Ruff et al. [8] applied a gravimetric method combined with a chromatography technique to measure the solvent sorption of those systems. The gravimetric information was used to determine the total mass of solvents in the sample, while chromatographic methods were used to differentiate between the two solvents in the sample. Moreover, Yurekli et al. [9] utilised infrared spectroscopy to measure the simultaneous sorption of toluene and methanol in polyvinyl acetate (PVAC).

In the present study, we applied an alternative approach that combines dynamic vapour sorption (DVS) and Raman spectroscopy to analyse the composition of a two-solvent/polymer system. Raman spectroscopy is ubiquitously used to measure the composition of multi-solvent mixtures. [10,11] The combined DVS/Raman analytics has already been used to detect moisture-induced structural changes in amorphous materials, such as hydrate formation or crystallisation. [12, 13]

The literature describes several approaches for modelling sorption isotherms of single solvents in polymers or APIs [14–16]. However, much less is known about modelling the simultaneous sorption of two solvents in a polymer or an ASD. Yurekli et al. [9] used the Flory-Huggins model to predict co-sorption isotherms of both toluene and methanol in PVAC using parameters adjusted to the corresponding PVAC/toluene and PVAC/methanol subsystems. However, this prediction showed a high deviation between the modelled relative saturation (RS), defined as the ratio of a solvent partial pressure and its vapour pressure, and the experimentally determined one. Crowley et al. [17] modelled IND/PVP/water sorption isotherms applying a combined Flory-Huggins/Vrentas model, which reasonably agreed with experimental data, at least for low drug loads (DLs). However, larger deviations were observed at higher DLs.

Alternatively, equations of state (EoS) like PC-SAFT have often been used to describe solvent sorption in API/polymer systems. [18,19] An advantage of PC-SAFT is that it explicitly considers intermolecular interactions, such as the association between molecules, which is particularly important when considering systems containing water and/or alcohol. For example, using PC-SAFT, Prudic et al. [20] modelled the water sorption in a polyvinylpyrrolidone (PVP)/naproxen ASD. Deviations between model prediction and experimental sorption data could be explained by the recrystallisation of naproxen, which took place parallel to the water-sorption measurement.

EoS like PC-SAFT or the lattice fluid model (LF EoS) are well established for describing sorption phenomena in polymers in equilibrium states. [18,19,21] However, they cannot describe solvent sorption in polymers below their glass-transition temperature (T_g) (non-equilibrium state). To describe sorption isotherms in glassy polymer systems, De Angelis et al. combined several EoS models with the Non-Equilibrium Thermodynamics of Glassy Polymers (NET-GP) approach to accurately describe the sorption isotherms of various single penetrants in glassy polymers. [22,23] This approach was initially developed to calculate sorption isotherms of gases in glassy polymers and was later also applied to vapours. An example is the work of SARTI et al. [24], who successfully described the sorption of either water or ethanol in polycarbonate with a combined approach of the LF EoS and NET-GP, known as the NELF model. Other examples are the works of Borrmann et al. [25,26] and Grönniger et al. [27], who combined PC-SAFT and the NET-GP modelling approach to describe the water sorption isotherms of several polymer-based systems and achieved excellent predictions. The combined modelling approach of PC-SAFT and NET-GP is denoted as NE-PC-SAFT. [28]

The main advantages of these combined approaches are that they (1) can be extended to API/polymer/solvent as well as two-solvent/polymer systems and (2) consider both the rubbery and glassy nature of polymers. Minelli et al. [29] have already successfully described an extension of the NELF model to multicomponent systems to evaluate mixed-gas solubilities in glassy polymers. In the present study, we use the NE-PC-SAFT model to predict sorption isotherms in the ternary systems IND/PVPVA64/ethanol and PVPVA64/water/ethanol.

2. Experiments

2.1. Materials

Poly(vinylpyrrolidone-co-vinyl-acetate) (PVPVA64) was purchased from BASF (Ludwigshafen, Germany) with a weight average molar mass of 65000 g mol^{-1} and IND from TCI (France) with a purity greater than 98 %. Ethanol (LiChroSolv) was obtained from Merck (Darmstadt, Germany) with a purity greater than 99.9 %. To generate deionised and filtered water, a Millipore® purification system from Merck was used.

2.2. ASD powder blends production

To prepare homogeneous ASD powder blends, PVPVA64 and IND were mixed in a Fritsch ball mill (Idar-Oberstein, Germany). The ball mill speed was set to 3000 rpm for three mixing cycles, each lasting three minutes, with a one-minute break between two cycles. The homogeneity of the ASD power blends was verified by Raman spectroscopy of ASD films prepared from the ASD power blends, as described in Section 2.3.

2.3. Film preparation

A vacuum compression moulding (VCM) device (MeltPrep GmbH) was used to prepare films of PVPVA64 and IND/PVPVA64 ASDs. The ASD or PVPVA64 films were cast on a thin aluminium plate (diameter 14 mm). First, the aluminium plate was placed into a round VCM geometry. The aluminium plate served as a substrate to prevent the fragile polymer or ASD films from breaking. Then, 10 mg of PVPVA64 or ASD powder was placed on the aluminium plate with a poly(tetrafluoroethylene) (PTFE) separation foil on top. In the following, the VCM geometry was heated up to 173 °C for 7 min under vacuum to melt the PVPVA64 onto the aluminium plate. The ASD powder was heated for 7 min to 153 °C under a vacuum. After this, the molten PVPVA64 or ASD films were cooled for 10 min on a cooling plate with a vacuum still applied. Afterwards, the films were removed from the VCM geometry and cooled to room temperature. Finally, the separation foil was released from the films with a razor blade. The mass of the films was determined by weighting using a precision balance from Mettler Toledo (± 0.01 mg) minus the mass of the aluminium plate.

IND films were produced using a thin film preparation method to minimise the influence of IND recrystallisation during the sorption measurement, as described in Section 4.1 in more detail. A Mettler Toledo high precision balance (± 0.001 mg) was used for sample weighing. For film preparation, 0.01to0.7 mg IND was placed on an aluminium plate and melted on a hotplate at 160 °C for 2 min with a PTFE foil on top. During melting, IND was distributed with a roller, generating an ultra-thin, homogenous film. After melting, the films were cooled down for 10 min to room temperature. Lastly, the separation foil was removed, analogous to the above mentioned ASD film production.

2.4. Absorption and desorption of either water or ethanol in PVPVA64, IND or ASDs

A DVS device (DVS Resolution, London, United Kingdom) from Surface Measurement Systems was used to measure the sorption of ethanol or water in PVPVA64, IND, and the ASDs (IND/PVPVA64). Measurements were performed in duplicates, and average values are reported. Measurements for IND/water were compared with existing literature data from Andronis et al. [30].Nitrogen was used as a dry carrier gas with a flow rate of 50 mL min^{-1}. The water concentration in the vapour phase was controlled by adjusting the relative humidity (RH), and the ethanol concentration in the vapour phase was controlled by adjusting the RS. RH and RS were generated by mixing dry nitrogen

and solvent vapours in defined flow ratios. Films prepared as described in the previous section were weighted using the internal high-precision balance (accuracy ±0.1 μg). All measurements were conducted at 30 °C (±0.1 K).

As the first step, films of PVPVA64, IND or ASDs were dried in the DVS to remove residual water sorbed from the surrounding atmosphere. Sorption measurements were carried out starting from entirely dried films, i.e. when the sorption rate was lower than 0.5 μg/g/min.

Analogously, for the sorption measurements in the PVPVA64 and ASD films, fixed RHs or RSs were maintained until the sorption rates were lower than 0.5 μg/g/min. We stepwise investigated absorption intervals from 0 to 0.15; 0.15 to 0.3; 0.3 to 0.45; 0.4 to 0.5; 0.5 to 0.6; 0.6 to 0.7; 0.7 to 0.8; and 0.8 to 0.9 RH or RS. Inverse intervals of RH/RS were applied for the desorption measurements. When measuring the ethanol sorption in IND, a new IND film was used for each sorption step (0–0.15; 0–0.3; 0–0.45; 0–0.6; 0–0.75; and 0–0.9 RS) to decrease the chance for simultaneous sorption and recrystallisation. Due to the different IND film thicknesses (supplement S1), a time criterion was used for each of these sorption steps, ranging between 5 min for the thinnest and 2 h for the thickest films, making sure that sorption equilibrium was reached for each RS step.

To obtain the sorption isotherms, we calculated the corresponding weight fractions of ethanol or water using the measured masses of the sample and of the dry PVPVA64, IND or ASD films.

2.5. Absorption and desorption of both water and ethanol in PVPVA64

The DVS device, as described in Section 2.3, was used to measure the simultaneous sorption of water and ethanol in PVPVA64. For that purpose, the DVS device was equipped with a Raman probe from i-Raman®Plus (B&W Tek) integrated into the sample chamber. For measurement, the Raman probe was placed 5 mm above the sample. The sample was exposed to the Raman laser (wavelength of 785 nm and laser intensity of 100 %) for seven seconds per measurement. Raman spectra were recorded as triplicates to optimise the signal-to-noise ratio. Additional information about the experimental setup and the measuring principle can be found in the literature. [31]

First, Raman spectra of the pure substances PVPVA64 and ethanol and of PVPVA64/ethanol mixtures of known composition were recorded for calibration. The Raman spectra were analysed using the software tool PEAXACT (Aachen, Germany). We selected a wavenumber region from 500 to 1600 cm^{-1} for peak analysis, as water is known to have no characteristic peaks in this region. [32] Furthermore, there exist no peak shifts of PVPVA64 due to the hydrogen bonding between PVPVA64 and water in this wavenumber region. [33]

Mass fractions of ethanol and PVPVA64 were determined using Raman spectroscopy and then used to calculate the water mass fraction by closing the mass balance. Similar to the measurements of the single-solvent systems (Section 2.4), the PVPVA64 films were dried in the DVS before being subjected to the mixed water/ethanol vapour. Table 4 (Section 4.3) lists the corresponding RH and RS values. Raman spectra were recorded in sorption equilibrium, assumed when the sorption rate became lower than 0.5 μg/g/min.

3. Modelling

3.1. Calculation of sorption isotherms

The thermodynamic condition for the equilibrium between a polymer or an ASD (the liquid phase) and the surrounding vapour phase is defined via the equality of the fugacities of water and ethanol in the liquid phase (f_i^L) and in the vapor (f_i^V) phase according to Eqs. (1a) and (1b)

$$f_i^L\left(T,p,V^{EQ}(T,p),x_i\right)=f_i^V(T,p);\quad if\quad x_i^{NE}>x_i^{EQ} \tag{1a}$$

$$f_i^L\left(T,p,V^{NE},x_i\right)=f_i^V(T,p);\quad if\quad x_i^{NE}\le x_i^{EQ} \tag{1b}$$

In Eq. (1a), f_i^L denotes the fugacity of water or ethanol in the rubbery amorphous phase (polymer or ASD), evaluated at the equilibrium volume V^{EQ} at system temperature T and pressure p. f_i^V at the same conditions is equivalent to the partial pressure p_i of water or of ethanol in the vapour phase. In a glassy system, the volume relaxation takes significantly longer than in the rubbery state. Thus, the solvents are assumed to be in a pseudo-equilibrium between the glassy system and the vapour phase. In Eq. (1a), f_i^L represents the fugacity of water or ethanol in the glassy amorphous phase (polymer or ASD), evaluated at the non-equilibrium volume (V^{NE}) calculated from Eq. (5). The transition from Eq. (1a) to Eq. (1b) is defined to take place at the point were the water or ethanol mole fraction x_i^{EQ} equals the mole fraction x_i^{NE} in non equilibrium.

3.2. PC-SAFT

PC-SAFT was used to obtain the fugacities of water or ethanol in the rubbery and glassy amorphous phases in Eqs. (1a) and (1b). PC-SAFT calculates the reduced Helmholtz residual energy a^{res} of a system using Eq. (2). [18,19]

$$a^{res}=a^{hc}+a^{disp}+a^{assoc} \tag{2}$$

The residual Helmholz energy consists of three contributions: the one for the hard-chain reference fluid (a^{hc}), the one for dispersion (a^{disp}), and the association contribution (a^{assoc}). The contribution for the hard chain a^{hc} accounts for the volume of the molecules via the segment diameter σ_i and the segment number m_i^{seg}. The dispersion contribution, a^{disp}, considers the van-der-Waals attraction forces between the molecules, whereas $\frac{u_i}{k_B}$ is used as an dispersion energy parameter and a^{assoc} takes into account hydrogen bonding via the association-energy parameter $\frac{\epsilon^{AiBi}}{k_B}$, the-association volume κ^{AiBi} and the number of accociation cites N^{assoc}.

To model mixtures, Berthelot-Lorenz mixing rules are applied to calculate the segment diameter σ_{ij} and the dispersion-energy parameter $u_{ij}\ /k_B$, whereas the Wolbach-Sandler mixing rules were used to calculate the cross-association volume κ^{AiBj} and the cross-association energy ε^{AiBj}. [34–36] Two binary interaction parameters k_{ij} and k_{ij}^{HB} were used in this work. The parameter k_{ij} corrects for the dispersion energy in the mixture, whereas k_{ij}^{HB} corrects the cross-association energy in the mixture (Eqs. 3 and 4) [37].

$$u_{ij}=\sqrt{u_i u_j}\ \left(1-k_{ij}\right) \tag{3}$$

$$\varepsilon^{AiBj}\ =\ 0.5\left(\varepsilon^{AiBi}+\varepsilon^{AjBj}\right)\ \left(1-k_{ij}^{HB}\right) \tag{4}$$

The PC-SAFT pure-component parameters of IND, PVPVA64, water, and ethanol were taken from the literature and are shown in Table 1. Binary interaction parameters of PC-SAFT (Table 2) (k_{ij} and k_{ij}^{HB}) were

Table 1
Pure-component parameters of PC-SAFT and NET-GP of the compounds investigated in this work.

	PVPVA64 [38]	*Ethanol* [19]	*Water* [39]	*IND* [40]
M_i/g mol^{-1}	65000	46.069	18.02	357.79
m_i/M_i mol g^{-1}	0.0372	0.0517202	0.06687	0.03992
σ_i/Å	2.947	3.1771	2.947	3.535
u_i/k_B / K	205.271	198.24	353.94	262.791
ϵ^{AiBi}/k_B / K	0	2653.4	2425.67	886.4
κ^{AiBi} / -	0.02	0.032384	0.0451	0.02
N_i / -	653/653	1/1	1/1	3/3
v_{0p}^{NE} / $cm^3\ g^{-1}$	0.7937 (*)	—	—	—

(*) Parameter determined within this study.

fitted to the water and ethanol-sorption isotherms, shown in Figs. 1 and 3, which will be discussed in Sections 4.1 and 4.2.

3.3. NET-GP

For modelling glassy systems, PC-SAFT was combined with NET-GP, denoted as NE-PC-SAFT. The volume of a system in the glassy state, which is a non-equilibrium state (NE), differs from the equilibrium (EQ) volume calculated by PC-SAFT.

The non-equilibrium volume was calculated using Eq. (5) in analogy to the work of Minelli et al. [29] for gaseous penetrant mixtures.

$$\frac{V_0^{NE}}{V^{NE}} = \frac{v_0^{NE}}{v^{NE}}\left(w_p + w_a\right) = 1 - \sum_{i=w,e}\left(k_{sw,i}\cdot\frac{p_i}{p_{0i}^{LV}}\right) \tag{5}$$

Here, V_0^{NE} is the volume of the dry ASD in non-equilibrium and V^{NE} denotes the non-equilibrium volume of the ASD/solvent(s) systems. The parameters v_0^{NE} and v^{NE} are the corresponding specific volumes. w_p is the weight fraction of the polymer (PVPVA64) and w_a the weight fraction of the API (IND). $k_{sw,i}$ is the swelling coefficient of the ASD by water or ethanol and p_i and p_{0i}^{LV} are the water and ethanol partial pressures and vapour pressures, respectively. For water, the ratio of p_i and p_{0i}^{LV} is called RH and for ethanol, RS. The specific dry volume of the ASD, v_0^{NE} was calculated by applying the mixing rule in Eq. (6).

$$v_0^{NE} = DL\cdot v_{0a}^{NE} + (1 - DL)\cdot v_{0p}^{NE} \tag{6}$$

In Eq. (6) v_{0p}^{NE} and v_{0a}^{NE} denote the specific volumes of the dry polymer and the dry API in non equilibrium. *DL* describes the drug load, given as $w_a/\left(w_p + w_a\right)$.

The swelling coefficients $k_{sw,i}$ of the ASD by water or ethanol are obtained via mixing rules according to Eq. (7).

$$k_{sw,i} = \frac{v_{0a}^{NE}}{v_0^{NE}}\cdot DL\cdot k_{sw,i}^{a} + \frac{v_{0p}^{NE}}{v_0^{NE}}\cdot(1 - DL)\cdot k_{sw,i}^{p} \tag{7}$$

Here, $k_{sw,i}^{p}$ are the swelling coefficients of the polymer and $k_{sw,i}^{a}$ of the API by the solvent i being either water or ethanol. *DL* denotes the drugload. The specific dry volume of the ASD, the polymer and the API are denoted as v_0^{NE}, v_{0p}^{NE} and v_{0a}^{NE}, respectively.

The non-equilibrium volume v_{0p}^{NE} and swelling coefficients $k_{sw,i}^{p}$ were fitted to the regions of the water-sorption and ethanol-sorption isotherms where the polymer-solvent mixtures behave glassy (Sections 4.1 and 4.2) and are listed in Table 2.

3.4. Modeling the glass-transition temperatures

The glass transitions were modelled using the Gordon-Taylor equation (Eq. (8)) [43]. w_i are the mass fractions of the individual components. The Gordon-Taylor parameters K_i were calculated using the Simha-Boyer rule [44] (Eq. (9)) using the pure-component glass--transition temperatures $T_{g,0i}$ and densities ρ_{0i}. The density of the polymer is denoted as $\rho_{polymer}$ and the polymer glass transition as $T_{g,polymer}$. Table 3 summarizes the pure-component data used in this work. For IND/water, $K_i = 9.091$ was taken from Andronis et al. [30]

Table 2
Binary interaction parameters of PC-SAFT and NET-GP used in this work.

	k_{ij}	k_{ij}^{HB}	$k_{sw,i}^{p}$
PVPVA64/Ethanol	0.00267 (*)	0.45521 (*)	0.031 (*)
PVPVA64/Water	−0.128 [25]	—	0.00001 (*)
Water/Ethanol	−0.0382 [41]	—	—
IND/Ethanol	−0.001 (*)	—	—
IND/Water	−0.022 [42]	—	—
PVPVA64/IND	−0.0621 [24]	—	—

(*) Parameter determined within this study.

$$T_g = \frac{\sum_i K_i w_i T_{g,0i}}{\sum_i K_i w_i} \tag{8}$$

$$K_i = \frac{\rho_{polymer} T_{g,polymer}}{\rho_{0i} T_{g,0i}} \tag{9}$$

4. Results and discussion

Sorption isotherms presented in the following sections describe the concentration of volatile compounds (VC) in pharmaceutical products (PVPVA64, IND, or an IND/PVPVA64 ASD) as a function of RH and/or RS at a constant temperature of 30 °C in the equilibrium state. Volatile compounds considered in this work are ethanol and water. Desorption measurements will be discussed for all PVPVA64-containing systems, whereas absorption measurements for IND/water and IND/ethanol. This was done to minimise the risk of recrystallisation of the amorphous IND (desorption measurements take much longer). Modelling the sorption isotherms was performed by applying a combined approach of PC-SAFT and NET-GP, denoted as NE-PC-SAFT (Section 3.3).

4.1. Sorption of ethanol in PVPVA64, IND, or ASDs

Ethanol sorption isotherms of PVPVA64, IND, and ASDs (IND/PVPVA64) were measured as described in Section 2.4 (Fig. 1(a)). Respective sorption data are tabulated in supplement S2. The ethanol sorption isotherm of IND shows a characteristic increase in ethanol mass fraction with increasing RS (convex shape). In contrast, the ethanol sorption isotherm of PVPVA64 shows a more sigmoidal shape. For RS lower than 0.8, the equilibrium ethanol mass fractions in PVPVA64 are lower than those in IND. For example, at RS=0.3, PVPVA64 absorbs approximately three times as much ethanol as IND. Conversely, at an RS higher than 0.8, the ethanol equilibrium mass fraction in IND exceeds the one of PVPVA64. The ethanol-sorption isotherm of the ASD (DL=0.1) shows a similar shape to the ethanol-sorption isotherm of PVPVA64, whereby the presence of IND reduces the ethanol uptake compared to the pure polymer (Fig. 1(a)).

It is crucial to emphasise that the IND films for measuring the ethanol sorption isotherms were produced using the thin film preparation technique described in Section 2.3. This was necessary as IND tends to recrystallise even at low RS of ethanol, which results in an overlapping of the ethanol-sorption kinetics with the IND crystallisation kinetics. The amorphicity of the films was verified by microscopic analysis. Sample images are provided in supplement S3.

Crystallisation kinetics are connected to molecular mobility and thus directly related to wet T_g. Consequently, ethanol sorption in the amorphous IND causes an increase in molecular mobility, promoting IND crystallisation during ethanol sorption. [52] IND crystallisation, in turn, influences ethanol sorption, as shown for the RS interval from 0 to 0.45 in Fig. 1(b). Here, after an initial increase in mass due to ethanol sorption, a drastic decrease in ethanol mass fraction was observed after approximately 5 min (curve I, Fig. 1(b)). This is because IND crystallised and crystalline IND absorbs much less ethanol than amorphous IND.

These findings are consistent with crystal formation observed via light microscopy after 10 min of ethanol sorption (Fig. 2(a)) and the literature-known recrystallisation of amorphous IND at 30 °C in an ethanol-containing atmosphere. [53,54]

As shown in Fig. 1(b), a substantial reduction of the film thickness from 9.9 µm (curve I) to 1.7 µm (curve II) enabled reaching the sorption equilibrium before substantial crystallisation occurred. Here, the maximum ethanol uptake of the IND film with a thickness of 1.7 µm is higher than that of the film with a thickness of 9.9 µm. Moreover, for the thinner film (Fig. 1(b), curve II), the sorption equilibrium is reached after about five minutes, while recrystallisation only begins after 20 min.

Microscopic images taken after ten minutes of starting the sorption measurement confirm almost complete elimination of recrystallisation

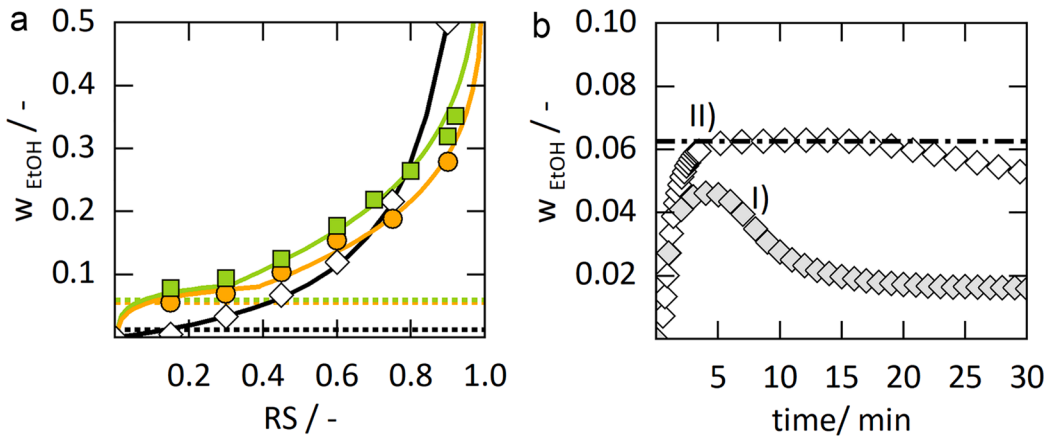

Fig. 1. (a) Ethanol sorption isotherms as a function of ethanol RS at 30 °C in PVPVA64 (squares, desorption), IND (diamonds, absorption), and in an ASD (IND/PVPVA64) with DL=0.1 (circles, desorption). Sorption isotherms modelled with NE-PC-SAFT are shown as solid lines. Ethanol weight fractions at the glass transition at 30 °C, calculated using the Gordon-Taylor equation, are indicated as dotted lines for PVPVA64/ethanol, ASD/ethanol, and IND/ethanol (from top to bottom; the first two are almost identical). (b) Ethanol-sorption in IND at 30 °C as a function of time for an RS step from 0 to 0.45. Grey diamonds indicate an IND film thickness of 9.9 μm, while white diamonds indicate an IND film thickness of 1.7 μm. The sorption equilibrium at RS=0.45 is visualised as a dash-dotted line.

Table 3
Glass-transition temperatures and densities of the substances used in this work.

Substance	$T_{g,0i}$ / K	ρ_{0i}/ g cm^{-3}
IND	317.6 [45]	1.32 [46]
PVPVA64	383 [47]	1.19 [48]
Water	136 [49]	1.0
Ethanol	97 [50]	0.78 [51]

via reducing film thickness. Only isolated small crystallisation nuclei became visible (Fig. 2(b)). Consequently, the ethanol sorption isotherm of amorphous IND, as represented in Fig. 1(a), becomes measurable by speeding up the sorption through a drastic reduction of film thickness. For the modelling, we therefore used the ethanol sorption data for thin IND films, ensuring that ethanol sorption was equilibrated before substantial crystallisation occurred. The film thicknesses used to measure the individual ethanol sorption intervals can be found in Table 6 of supplement S1.

The NE-PC-SAFT approach (Section 3.1) was used for modelling the ethanol sorption isotherms of PVPVA64 and IND. Fig. 1(a) shows an excellent agreement between model fitting and experimental data for all RS ranges and both the glassy and rubbery states. The absolute average deviation (AAD) in ethanol mass fractions is 0.016 for PVPVA64/Ethanol and 0.004 for IND/Ethanol. As fitting parameters, we used the binary interaction parameters k_{ij}, k_{ij}^{HB} of PC-SAFT and $k_{sw,i}^{p}$ and v_{0P}^{NE} from the NET-GP approach (Tables 1 and 2). The intersection between the two model approaches (PC-SAFT and NE-PC-SAFT) for the ethanol sorption of PVPVA64 is shown as a kink, located approximately at an ethanol mass fraction of 0.09. It is noticeable that this intersection point is close to the glass transition of the wet polymer predicted using the Gordon-Taylor equation (Fig. 1). This is reasonable because, as outlined in Section 1, the NET-GP approach was explicitly developed to model sorption isotherms in glassy polymers. The obtained non-equilibrium dry density of PVPVA64 applying the NET-GP approach (1.26 g/cm^3), which is the reciprocal of v_{0P}^{NE} (Table 1), is close to the true density of PVPVA64 (1.19 g cm^3) reported in the literature. [48] This confirms that this model parameter is physically meaningful. The obtained swelling coefficient of PVPVA64 by ethanol ($k_{sw,i}^{p}$Table 2) is quite small. We, therefore, explain the ethanol sorption of PVPVA64 in the glassy region being dominated by pore penetration of ethanol in PVPVA64 and only a low impact of swelling.

Based on the model parameters fitted to the ethanol sorption isotherms of IND and PVPVA64, the ethanol sorption isotherm of an ASD (IND/PVPVA64) with DL 0.1 was purely predicted using the NE-PC-SAFT approach. As shown in Fig. 1(a), the model prediction and the

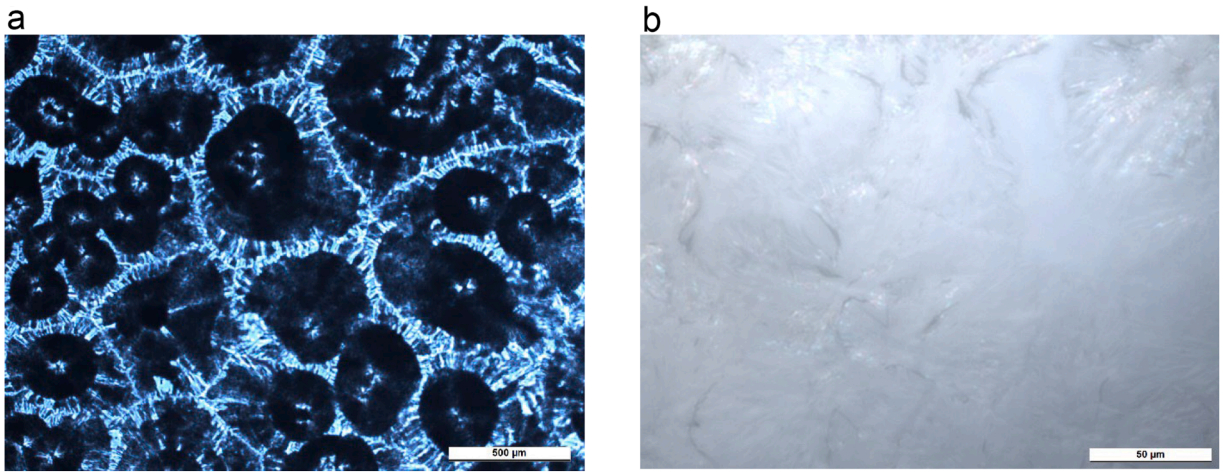

Fig. 2. Microscopic images of IND crystal formation after an ethanol sorption measurement for an RS step between 0 and 0.45 at 30 °C (sorption data shown in Fig. 1 (b)) taken after 10 min sorption measurement (a) IND film of 9.9 μm thickness. (b) IND-film of 1.7 μm thickness.

experimental data are in excellent agreement for the whole ethanol RS range with an AAD in ethanol mass fraction of only 0.012.

4.2. Sorption of water in PVPVA64 or IND

Fig. 3 displays the water sorption isotherms of PVPVA64 and IND at 30 °C. These data were obtained via absorption/desorption interval measurements in the DVS, as described in Section 2.4 and are provided in supplement S4.

The measured water-sorption isotherm of PVPVA64 shows a non-linear shape with an increase in the slope with increasing RH. In contrast, the water sorption in IND is much lower than in PVPVA64 for the whole RH range. For a given RH, PVPVA64 absorbs significantly more water than IND. For example, at an RH of 0.6, the mass fraction of water in PVPVA64 is 0.116, whereas the water mass fraction in IND is 0.012, approximately ten times less than that of water in PVPVA64. The higher sorption capacity of PVPVA64 can be explained by its hydrophilic nature in contrast to the very hydrophobic IND. For the water sorption in IND, only very low water mass fractions are obtained at RH close to 1. This indicates the occurrence of liquid-liquid-equilibrium (LLE) in the IND/water system. At 30 °C, we predicted an LLE between IND and water with water mass fractions of 0.029 and 0.999 in the two phases. This perfectly fits the experimental VLE data shown in Fig. 3, indicating a liquid-liquid-vapour three-phase equilibrium at an RH close to 1. [55] Overall, the measured water sorption isotherm of IND shows an excellent agreement with existing literature data from Andronis et al. [30] with a mean deviation of only 3.5 %.

The sorption isotherms were again modelled using the NE-PC-SAFT approach. PC-SAFT parameters were taken from previous studies by Borrmann et al. [25,42]. Whereas above T_g, the same sorption equilibrium is reached for both absorption and desorption, there is a hysteresis effect below the glass transition (see supplement S5). In order to account for this hysteresis, NET-GP parameters for systems containing PVPVA64 were adjusted to the desorption data (Fig. 3). Fig. 3 shows a very good agreement between model fit and the experimental water desorption data. The AAD in water mass fractions is 0.04 for PVPVA64/water and 0.0012 for IND/water.

For the water sorption isotherm of PVPVA64, the transition between the modelling with PC-SAFT (Eq. (1a)) and the NE-PC-SAFT approach (Eq.(1b)) is again close to the water mass fraction at T_g predicted using the Gordon-Taylor equation, which underlines the physical significance of our modelling approach. Consequently, PVPVA64 becomes rubbery

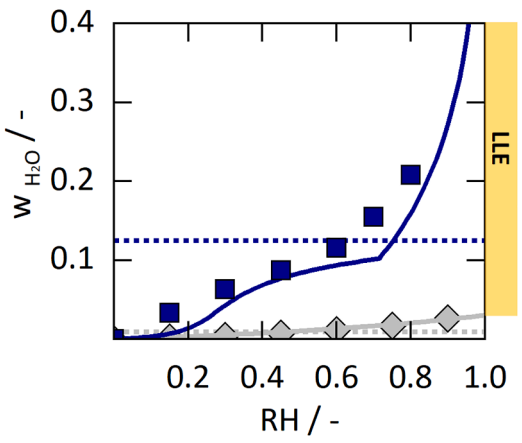

Fig. 3. Water sorption isotherms as a function of RH at 30 °C of PVPVA64 (squares, desorption) and IND (diamonds, absorption). PC-SAFT/NET-GP modelled sorption isotherms are shown as solid lines. The bar on the right-hand side indicates that PC-SAFT predicted liquid-liquid phase separation (LLE) of IND/water. Water-weight fractions at the glass transition of 30 °C, as calculated using the Gordon-Taylor equation, are indicated as dotted lines for PVPVA64/water and IND/water (from top to bottom).

for sorbed water mass fractions higher than 10 wt %. This is because the sorbed water drastically decreases the polymer glass transition due to the plasticising effect of water. Again, the adjusted NET-GP model parameters are in a physically reasonable order of magnitude using the same v_{0P}^{NE} as described in Section 4.1. and a negligible swelling coefficient of water in PVPVA64 ($k_{sw,i}^{p}$ Table 2). This small swelling can be explained by the antiplasticizing impact of water on PVPVA64. [25] Due to this, an additional free volume becomes available for water diffusion in the glassy polymer. Water diffusion can, therefore, be assumed to be the dominating effect, whereas polymer swelling can be neglected. Water-sorption isotherms of IND/PVPVA64 ASDs can be predicted analogously to the ethanol-sorption isotherms (Section 4.1). This has already been shown in previous works of our group [26,56].

4.3. Co-sorption of water and ethanol in PVPVA64

If the vapour phase contains ethanol and water (collectively referred to as volatile compounds, VCs), PVPVA64 absorbs both of them simultaneously. The experimental data of these co-sorption isotherms are listed in Table 4.

Fig. 4 shows the co-sorption of ethanol and water in PVPVA64 at constant RH levels over the whole range of investigated RS, measured as described in Section 2.5. Fig. 4(a) shows the overall VC sorption in PVPVA64, and Fig. 4(b) the one of ethanol (at different RHs). The experimental data in Fig. 4(a) show an increase in overall VC sorption with an increase in RH. Fig. 4(b) shows that the ethanol sorption is almost independent of RH at low RS of ethanol (RS < 0.3). At higher RS, ethanol sorption increases with increasing RH levels (0; 0.3 and 0.5). This means that the presence of water enhances the ethanol sorption in PVPVA64.

Using the parameters determined above by fitting the sorption data of the single solvents in PVPVA64 (Tables 1 and 2), the NE-PC-SAFT approach was able to predict the ethanol/water co-sorption in PVPVA64 in almost quantitative agreement with the experimental data. This applies to the concentration of both VCs (Fig. 4(a)) and ethanol (Fig. 4(b)).

Fig. 5 presents the sorption equilibrium data shown in Fig. 4 in a ternary phase diagram to differentiate between the mass fractions of the individual components (water, ethanol, and PVPVA64) in the polymer sample.

The measured water mass fractions absorbed in PVPVA64 in the presence of ethanol are almost independent of the ethanol content as long as the samples are in the rubbery state. This means that the water concentration in the polymer depends on RH but is less influenced by RS. In contrast, the ethanol equilibrium concentrations in PVPVA64 increase upon increasing both RS and RH. As a result, the ethanol concentration in the polymer increases with increasing water concentration in the sample (increasing RH), even for constant RS. This means that the presence of water promotes additional ethanol sorption of PVPVA64, while the opposite does not apply.

This can be explained by the different cross-association energies in the systems ethanol/water ($3.51 \cdot 10^{-20}$J), PVPVA64/water ($1.67 \cdot 10^{-20}$J) and PVPVA64/ethanol ($9.98 \cdot 10^{-21}$J) calculated from PC-SAFT. The association energy between water and ethanol is about 3.5 times that between ethanol and PVPVA64. This means that larger amounts of water in PVPVA lead to an increase in ethanol sorption compared to the water-free system.

The phase diagram shows the transitions between modelling with PC-SAFT and the NE-PC-SAFT approach as kinks in the calculated isoRH and isoRS lines. Qualitatively, the experimental data align with the kinking of the isoRH lines at the transition from the rubbery to the glassy state. The Gordon-Taylor predicted concentration line at T_g= 30 °C also agrees approximately with the line of intersection points of the two model approaches.

The model predictions of the ethanol/water co-sorption isotherms

Table 4
Water and ethanol co-sorption data in PVPVA64 at 30 °C (±0.1 K) for different RH and RS values. The sample masses were weighed with ±0.1 μg accuracy, and the RH/RS was adjusted with an accuracy of ±0.5 %.The measurement uncertainty is ±4.1 %.

Measurement 1	***RH***	0.3	0.3	0.3	0.3	0.3	0.3
	RS	0.5	0.4	0.3	0.2	0.1	0
	w_{H2O}	0.027	0.024	0.02	0.020	0.015	0.031
	w_{EtOH}	0.182	0.144	0.112	0.081	0.065	0.022
Measurement 2	***RH***	0.5	0.5	0.5	0.5	0.5	0.5
	RS	0.5	0.4	0.3	0.2	0.1	0
	w_{H2O}	0.058	0.058	0.057	0.057	0.048	0.059
	w_{EtOH}	0.220	0.167	0.123	0.086	0.066	0.024

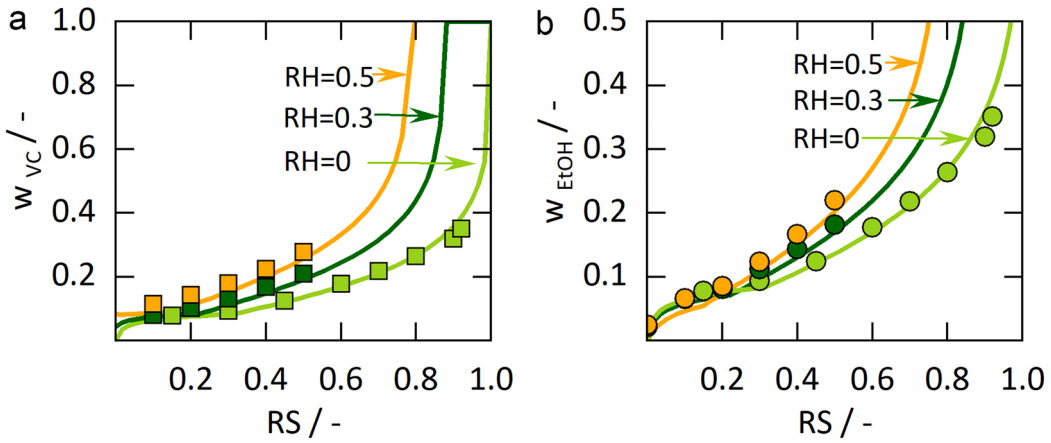

Fig. 4. Ethanol/water co-sorption isotherms of PVPVA64 at 30 °C for three different RHs and varying RS (desorption). The measured co-sorption data are displayed as squares for overall VC weight fraction (a) and as circles for ethanol weight fractions in the polymer (b). NE-PC-SAFT modelled co-sorption isotherms are shown as solid lines.

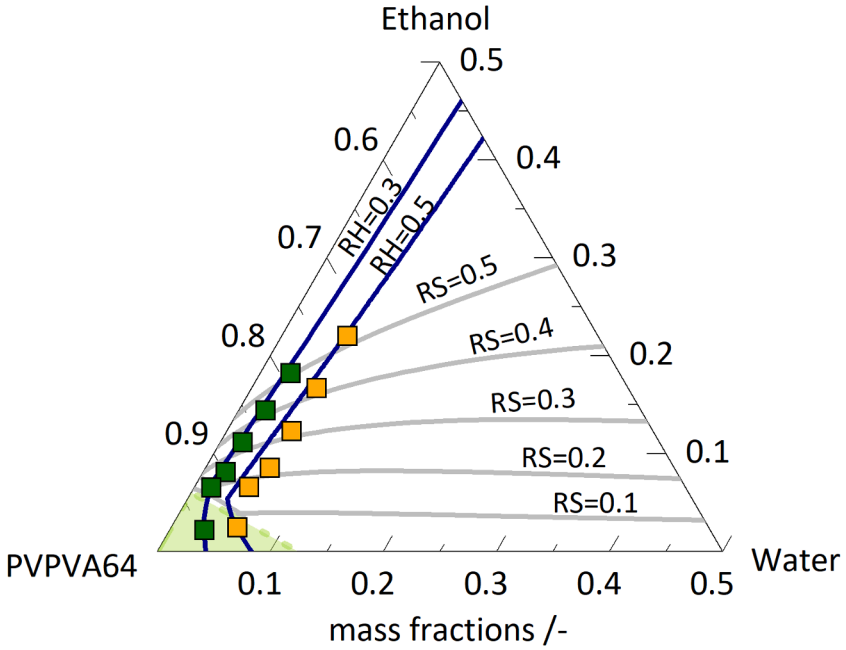

Fig. 5. Phase diagram of PVPVA64, ethanol, and water at 30 °C. Experimental vapour-sorption data at a constant RH are displayed as squares. Blue solid lines from left to right are NE-PC-SAFT predicted isohumidity lines, i.e. equilibrium compositions in the polymer sample established at the indicated RHs. Analogously, grey solid lines from top to bottom represent NE-PC-SAFT-predicted lines at constant RS. The green glass-transition line predicted using the Gordon-Taylor equation limits the green area where the system is in the glassy state (left corner).

applying the NE-PC-SAFT approach Eqs. (1a) and (1b) very well align with the experimental data in both the glassy and rubbery regions (Fig. 5). For perfect agreement between the prediction and experiment, the experimentally determined weight fractions of ethanol and water at fixed RS and RH should be found at the predicted intersections of the isoRH and isoRS lines. As can be seen, the positions of the NE-PC-SAFT predicted intersection points almost perfectly match the experimental data. The calculated AAD for ethanol and water mass fractions in the

saturated PVPVA64 sample was 0.011 for water and 0.023 for ethanol. It is again worth noting that none of the model parameters was fitted to the co-sorption data shown in Figs. 4 and 5.

4. Conclusion

This paper presented a methodology for measuring ethanol sorption isotherms of amorphous IND via DVS by utilising ultra-thin IND films. This enabled rapid sorption equilibration before significant recrystallisation of the amorphous IND occurred. To the best of our knowledge, ethanol-sorption isotherms of amorphous IND have not yet been measured in the literature due to the high recrystallisation potential of IND in an ethanol-containing atmosphere. The ethanol sorption in an ASD of IND and PVPVA64 at 30 °C was predicted using an NE-PC-SAFT modelling approach in almost quantitative agreement with experimental data. For this purpose, model parameters were only fitted to the ethanol-sorption data in either PVPVA64 or IND.

Furthermore, this study investigated the water/ethanol co-sorption isotherms of PVPVA64 as an example of a two-solvent/polymer system. Experimental data were obtained by coupling vapour-sorption measurements with Raman spectroscopy to analyse the resulting liquid composition. The NE-PC-SAFT approach predicted the water/ethanol co-sorption in PVPVA64 at two distinct RH and six different RS levels of ethanol in very good agreement with the experimental data using the same parameters as for the single-solvent sorptions of water and ethanol in PVPVA64. Remarkably, even the predicted liquid compositions for the glassy state are in agreement with the experimental findings.

We were able to show that the NE-PC-SAFT approach is able to predict sorption/co-sorption isotherms of polymer-based formulations like IND/PVPVA64. This significantly reduces the experimental workload to characterise ASD formulations and provides a framework for process development in solvent-based manufacturing methods. In addition to sorption equilibria, diffusion coefficients are essential to design ASD drying processes. They will be the subject of a subsequent work.

CRediT authorship contribution statement

Jana Kerkhoff: Writing – original draft. **Dominik Borrmann:** Writing – original draft. **Gabriele Sadowski:** Writing – original draft.

Declaration of competing interest

The authors declare the following financial interests/personal relationships which may be considered as potential competing interests:

Jana Kerkhoff reports financial support was provided by INVITE GmbH. If there are other authors, they declare that they have no known competing financial interests or personal relationships that could have appeared to influence the work reported in this paper.

Data availability

Data will be made available on request.

Acknowledgement

The authors thank the Drug Delivery Innovation Center (DDIC), Invite GmbH, Leverkusen for financial support.

Supplementary materials

Supplementary material associated with this article can be found, in the online version, at doi:10.1016/j.fluid.2024.114247.

References

[1] P.S. Jagtap, R.R. Tagad, R.S. Shendge, J. Drug Delivery Ther. 9 (2019) 493–500.
[2] T. Vasconcelos, B. Sarmento, P. Costa, Drug Discov. Today 12 (2007) 1068–1075.
[3] T. Vasconcelos, S. Marques, J. das Neves, B. Sarmento, Adv. Drug Deliv. Rev. 100 (2016) 85–101.
[4] S. Dohrn, C. Luebbert, K. Lehmkemper, S.O. Kyerematen, M. Degenhardt, G. Sadowski, Eur. J. Pharm. Biopharm. 158 (2021) 132–142.
[5] S. Dohrn, P. Reimer, C. Luebbert, K. Lehmkemper, S.O. Kyerematen, M. Degenhardt, G. Sadowski, Mol. Pharm. 17 (2020) 2721–2733.
[6] C. Luebbert, D. Real, G. Sadowski, Mol. Pharm. 15 (2018) 5397–5409.
[7] D.C. Bonner, N.F. Brockmeier, Industr. Eng. Chem. Process Design Develop. 16 (1977) 180–186.
[8] W.A. Ruff, C.J. Glover, A.T. Watson, AIChe J. 32 (1986) 1948–1953.
[9] Y. Yurekli, S.A. Altinkaya, Fluid. Phase Equilib. 277 (2009) 35–41.
[10] I. Durickovic, Applications of molecular spectroscopy to current research in the chemical and biological sciences, M.T. Stauffer (Ed.), IntechOpen, 2016.
[11] J.R. Ferraro, Introductory raman spectroscopy, Elsevier Science, Burlington, 2012.
[12] A. Paudel, D. Raijada, J. Rantanen, Adv. Drug Deliv. Rev. 89 (2015) 3–20.
[13] M.P. Feth, J. Jurascheck, M. Spitzenberg, J. Dillenz, G. Bertele, H. Stark, J. Pharm. Sci. 100 (2011) 1080–1092.
[14] P.J. Flory, J. Chem. Phys. 10 (1942) 51–61.
[15] K.M. Krüger, G. Sadowski, Macromolecules. 38 (2005) 8408–8417.
[16] F. Mueller, S. Naeem, G. Sadowski, Ind. Eng. Chem. Res. 52 (2013) 8917–8927.
[17] K.J. Crowley, G. Zografi, J. Pharm. Sci. 91 (2002) 2150–2165.
[18] J. Gross, G. Sadowski, Ind. Eng. Chem. Res. 40 (2001) 1244–1260.
[19] J. Gross, G. Sadowski, Ind. Eng. Chem. Res. 41 (2002) 5510–5515.
[20] A. Prudic, Y. Ji, C. Luebbert, G. Sadowski, Eur. J. Pharm. Biopharm. 94 (2015) 352–362.
[21] I.C. Sanchez, R.H. Lacombe, J. Phys. Chem. 80 (1976) 2352–2362.
[22] M.G. de Angelis, G.C. Sarti, Annu Rev. Chem. Biomol. Eng. 2 (2011) 97–120.
[23] M.G. de Angelis, F. Doghieri, G.C. Sarti, B.D. Freeman, Desalination. 193 (2006) 82–89.
[24] G.C. Sarti, M.G. de Angelis, AIChe J. 58 (2012) 292–301.
[25] D. Borrmann, A. Danzer, G. Sadowski, Membranes 12 (2022).
[26] D. Borrmann, A. Danzer, G. Sadowski, Pharmaceutics. 14 (2022).
[27] B. Grönniger, E. Fritschka, I. Fahrig, A. Danzer, G. Sadowski, Mol. Pharm. 20 (2023) 2194–2206.
[28] M.G. de Angelis, F. Doghieri, G.C. Sarti, B.D. Freeman, Desalination. 193 (2006) 82–89.
[29] M. Minelli, S. Campagnoli, M.G. de Angelis, F. Doghieri, G.C. Sarti, Macromolecules. 44 (2011) 4852–4862.
[30] V. Andronis, M. Yoshioka, G. Zografi, J. Pharm. Sci. 86 (1997) 346–351.
[31] F. Wolbert, K. Nikoleit, M. Steinbrink, C. Luebbert, G. Sadowski, Mol. Pharm. 19 (2022) 2483–2494.
[32] D.M. Carey, G.M. Korenowski, J. Chem. Phys. 108 (1998) 2669–2675.
[33] L.S. Taylor, F.W. Langkilde, G. Zografi, J. Pharm. Sci. 90 (2001) 888–901.
[34] D. Berthelot, Compt. Rendus 126 (1898) 15.
[35] H.A. Lorentz, Ann. Phys. 248 (1881) 127–136.
[36] J.P. Wolbach, S.I. Sandler, Ind. Eng. Chem. Res. 37 (1998) 2917–2928.
[37] Michael Bortz, Norbert Asprion (Eds.), Simulation and optimization in process engineering, Elsevier, 2022.
[38] K. Lehmkemper, S.O. Kyerematen, O. Heinzerling, M. Degenhardt, G. Sadowski, Mol. Pharm. 14 (2017) 157–171.
[39] L.F. Cameretti, G. Sadowski, in: Chemical engineering and processing: process intensification 47, 2008, pp. 1018–1025.
[40] A. Prudic, Y. Ji, G. Sadowski, Mol. Pharm. 11 (2014) 2294–2304.
[41] L.A. Ferreira, E.A. Macedo, S.P. Pinho, Chem. Eng. Sci. 59 (2004) 3117–3124.
[42] D. Borrmann, A. Danzer, G. Sadowski, Mol. Pharm. 19 (2022) 998–1007.
[43] M. Gordon, J.S. Taylor, J. Appl. Chem. 2 (1952) 493–500.
[44] R. Simha, R.F. Boyer, J. Chem. Phys. 37 (1962) 1003–1007.
[45] B.C. Hancock, G. Zografi, Pharm. Res. 11 (1994) 471–477.
[46] A. Prudic, T. Kleetz, M. Korf, Y. Ji, G. Sadowski, Mol. Pharm. 11 (2014) 4189–4198.
[47] M.S. Dudhedia, A.M. Agrawal, J. Appl. Polym. Sci. 133 (2016) n/a-n/a.
[48] K. Six, G. Verreck, J. Peeters, M. Brewster, G. van den Mooter, J. Pharm. Sci. 93 (2004) 124–131.
[49] A. Hallbrucker, E. Mayer, G.P. Johari, Philosoph. Magaz. Part B 60 (1989) 179–187.
[50] B. Kabtoul, M.A. Ramos, Physica Status Solidi (a) 208 (2011) 2249–2253.
[51] J.A. Dean, N.A. Lange, Lange's handbook of chemistry, 15th ed., McGraw-Hill, New York, 2001 [Distributed by] Knovel[Norwich, N.Y.]?
[52] B. Grönniger, E. Fritschka, K. Kimpe, A. Singh, G. Sadowski, Mol. Pharm. 21 (2024) 2908–2921.
[53] N. Hirota, Y. Hattori, M. Otsuka, Adv. Powder Techn. 27 (2016) 808–811.
[54] C.R. Malwade, H. Qu, Org. Process Res. Dev. 22 (2018) 697–706.
[55] S. Dohrn, C. Luebbert, K. Lehmkemper, S.O. Kyerematen, M. Degenhardt, G. Sadowski, Int. J. Pharm. 577 (2020) 119065.
[56] D. Borrmann, A. Danzer, G. Sadowski, Pharmaceutics. 14 (2022).